remote sensing

MDPI

Article

Estimating Regional Snow Line Elevation Using Public Webcam Images

Céline Portenier [1,2,*], Martina Hasler [1] and Stefan Wunderle [1,2]

[1] Institute of Geography, University of Bern, CH-3012 Bern, Switzerland
[2] Oeschger Centre for Climate Change Research, University of Bern, CH-3012 Bern, Switzerland
* Correspondence: celine.portenier@giub.unibe.ch

Abstract: Snow cover is of high relevance for the Earth's climate system, and its variability plays a key role in alpine hydrology, ecology, and socioeconomic systems. Measurements obtained by optical satellite remote sensing are an essential source for quantifying snow cover variability from a local to global scale. However, the temporal resolution of such measurements is often affected by persistent cloud coverage, limiting the application of high resolution snow cover mapping. In this study, we derive the regional snow line elevation in an alpine catchment area using public webcams. We compare our results to the snow line information derived from the Moderate-Resolution Imaging Spectroradiometer (MODIS) and Sentinel-2 snow cover products and find our results to be in good agreement therewith. Between October 2017 and the end of June 2018, snow lines derived from webcams lie on average 55.8 m below and 33.7 m above MODIS snow lines using a normalized-difference snow index (NDSI) of 0.4 and 0.1, respectively, and are on average 53.1 m below snow lines derived from Sentinel-2. We further analyze the superior temporal resolution of webcam-based snow cover information and demonstrate its effectiveness in filling temporal gaps in satellite-based measurements caused by cloud cover. Our findings show the ability of webcam-based snow line elevation retrieval to complement and improve satellite-based measurements.

Keywords: regional snow line elevation; public outdoor webcams; MODIS; Sentinel-2

Citation: Portenier, C.; Hasler, M.; Wunderle, S. Estimating Regional Snow Line Elevation Using Public Webcam Images. *Remote Sens.* **2022**, *14*, 4730. https://doi.org/10.3390/rs14194730

Academic Editors: Yubao Qiu and Ali Behrangi

Received: 29 June 2022
Accepted: 18 September 2022
Published: 21 September 2022

1. Introduction

Snow cover is highly variable, both spatially and temporally, and it is a crucial element of the Earth's climate system. Seasonal snow cover highly influences the radiation budget and water fluxes between the surface and the atmosphere, and it plays a significant role in the warming of the climate through snow–albedo feedback due to its high reflectance [1]. Mountain regions are particularly sensitive to changes in the extent of snow cover. Snow melt has a high impact on the availability of water resources and accounts substantially for the annual runoff generation in alpine catchment areas [2]. Moreover, changes in snow cover influence mountain ecology and socio-economic systems [3–5]. It is therefore essential to observe and analyze snow cover variability at a high spatiotemporal resolution.

Optical remote sensing is a measurement technique that is widely used to analyze snow-cover dynamics over large areas; see, e.g., [6–9]. In comparison to ground-based station measurements, satellite-based data can capture the spatial distribution of the snow extent. However, limitations exist in both spatial and temporal resolutions. For example, snow cover products generated from the Moderate Resolution Imaging Spectroradiometer (MODIS) can offer a daily coverage but a relatively low spatial resolution of 500 m [10]. On the contrary, Sentinel-2 snow cover maps provide a high spatial resolution of 20 m but only a 5-day revisit time [11]. Moreover, cloud cover has a high impact on observing snow dynamics since it can significantly limit the number of available scenes and the ability to accurately mapping snow cover extent using optical satellite data [12,13]. Spatial and temporal gap-filling methods are the most widespread methods used to reduce the impact

of cloud cover on data availability. However, these methods either are unable to remove all the cloud cover in large areas or introduce uncertainties that increase with the length of the data gaps [13,14].

Terrestrial photography is an observation method increasingly used to analyze snow cover variability at a high spatiotemporal resolution; see, e.g., [15–24]. Recently, ground-based cameras have been proposed to validate satellite-based snow cover information [25,26] and have been identified as a unique data set for precisely monitoring snow cover in mountainous regions [21,27,28]. Moreover, snow cover maps based on ground-based cameras have been used to continuously calibrate threshold values based on the Normalized Difference Snow Index (NDSI) for Landsat satellite images [29]. In contrast to satellite-based systems, ground-based cameras are typically able to monitor and detect features below cloud cover. In addition, the temporal resolution, or measurement interval, is practically unlimited. These reasons render measurements from ground-based cameras feasible for complementing satellite-based snow cover retrieval. Besides the studies presented by [22,28], the above mentioned studies focus on small-catchment areas, i.e., rely on a handful of cameras with only a limited areal coverage.

Public webcam images offer a significant potential to combine local-scale snow cover information at high spatio-temporal resolutions with an increased areal coverage due to their high availability. In Switzerland, for instance, several thousands of public webcams are freely accessible. Public webcams are less affected by cloud cover in comparison to camera networks covering small catchment areas, since the distribution of public webcams over larger areas enables a compensation of data gaps thanks to the spatial variability in cloud cover. Recently, the feasibility of using these webcams to retrieve snow cover information has been demonstrated [28].

This study builds on the work presented by Portenier et al. [28] with the purpose of highlighting the ability of public webcams to improve and complement satellite-based snow cover retrieval by contributing additional snow cover information. Between October 2017 and the end of June 2018, we studied the regional snow line elevation in an alpine catchment area using public webcams. The snow line, i.e., the transition between snow-covered and snow-free areas, is a suitable indicator to describe snow cover distribution in mountainous regions. We follow the definition and methodology proposed by Krajčí et al. [30], which define the Regional Snowline Elevation (RSLE) as the elevation for which the sum of snow pixels below and snow-free pixels above that elevation is minimized. Previous studies have already shown that terrestrial camera systems are an effective tool to monitor the variability in the snow line at small catchment scales [17,21]. We want to demonstrate that public webcams are an attractive and appropriate data source to estimate regional snow-line elevation at larger scales as well. The large number of public webcams enables us to analyze the temporal variability of the snow line over large areas. We compare snow-line elevation derived from webcams to snow-line estimates from existing MODIS and Sentinel-2 snow cover products and investigate their differences. In addition, we analyze the impact of cloud cover on data availability and demonstrate the feasibility to fill gaps in satellite-based snow cover time-series caused by cloudy conditions using webcams.

We first briefly describe the workflow to generate daily webcam-based snow cover maps (Section 2.1). Next, we create binary snow-cover data sets generated from daily MODIS Terra and Aqua snow-cover products and Sentinel-2 fractional snow-cover (FSC) maps provided by the NASA Distributed Active Archive Center at the National Snow and Ice Data Center (NSIDC) and the Copernicus Land Monitoring service (CLMS), respectively, (Section 2.2). In Section 2.3, the study area is described in detail, and the fraction observed by the webcams is put into context for the entire study area. In Section 2.4, we present the RSLE method proposed by Krajčí et al. [30]. A detailed analysis and comparison of the RSLE estimates derived from different measurements and the impact of cloud cover on the temporal resolution of the different data sets is presented in Section 3, followed by an in-depth discussion in Section 4.

2. Data and Methods

2.1. Webcam-Based Snow Cover Maps

We use public webcam images of 16 outdoor webcams located in the Swiss Alps. Most of the webcams are maintained by hotels, restaurants, and ski-lift operators and feature a view of the Swiss mountain landscape (see Figure 1 for some example images). Between October 2017 and the end of June 2018, webcam images were downloaded from the publicly accessible websites at an hourly interval, resulting in a total of 50,855 webcam images. Using a Unix-like environment, the command-line tool wget was used to download our images from the different web resources, and cron, a job scheduler on Unix-like operating systems, was used to automate this download process. For each webcam, the location was manually estimated using areal images on the mapping platform of the Swiss Confederation (map.geo.admin.ch (accessed on 28 June 2022)) and objects visible in the webcam image.

Figure 1. Example images of selected webcams (**a**) Aeschiried (© www.restaurantpanorama.ch (accessed on 24 March 2021)), (**b**) Lenk Hahnenmoos (© Lenk-bergbahnen.ch (accessed on 24 March 2021)), (**c**) Springenboden (© www.springenboden.ch (accessed on 24 March 2021)), (**d**) Kandersteg Bernerhof (© www.bernerhof.ch (accessed on 24 March 2021)), and (**e**) Kandersteg Sunnbüehl (© www.sunnbuel.ch (accessed on 24 March 2021)).

To generate daily snow-cover maps, the data set was reduced to a single image per webcam and day by automatically detecting images featuring high contrast and little cloud coverage that would hinder the view on the landscape. This was achieved by first applying Gaussian smoothing, followed by Canny edge detection to count the number of edges in each image. We assume that the higher the number of edges, the better the image contrast and the lower the probability of cloud occurrence in the webcam's field of view. For each day and webcam, we thus selected the image with the largest number of detected edges. If the largest number of detected edges was below a certain threshold, the image was tagged as cloud-covered. The daily measurement period was restricted to the time span between 7:00 and 16:00 local time (UTC+1) to exclude low-light conditions. The resulting data set consists of 3892 images in total, i.e., 14.3 images per day on average (1.7 images per day were unavailable due to webcam failure or missing archive data).

We used the automatic image-to-DEM registration approach proposed by Portenier et al. [28], which allows processing webcam images without having access to the webcams' intrinsic and extrinsic camera parameters. In addition, this registration process does not require manual user input, e.g., setting ground control points manually. Given a webcam image and an estimate of the webcam's location, the registration approach automatically resolves all required camera information (i.e., orientation and field of view of the camera) to project the pixel information onto a georeferenced map. This technique registers the mountain silhouette of a webcam image with the mountain silhouette of a rendered image of a high-resolution digital elevation model (DEM). For a certain set of camera parameters and viewing directions, a pinhole camera model projects the DEM's 3D points onto a 2D image plane of that camera and therewith generates virtual camera images of the landscape. We used the swissALTI^{3D} DEM with a spatial resolution of 2 m produced by the Swiss Federal Office of Topography [31] to perform the registration. The method iterates the most important camera parameters and considers the differences in cross-correlation between the webcam silhouette and the rendered silhouette to solve for the unknown camera parameters. The silhouette pair that maximizes cross-correlation yields the desired transformation matrix that relates pixel information of the webcam image to its

real-world coordinates. We refer to [28] for a detailed explanation of this image-to-DEM registration approach.

Since image-to-DEM registration is computationally intensive, we apply this method only once per webcam and apply automatic image-to-image alignment [28] to correct small camera movements and align all the webcam images with each other. Image-to-image alignment is about 20 to 30 times faster than image-to-DEM registration, depending on the resolution of the webcam image. It is based on Scale-Invariant Feature Transform (SIFT) features [32] and leverages the fitting model RANdom SAmple Consensus (RANSAC; [33]) to solve for the projective transformation induced by the shift of a webcam's orientation.

Next, we classified snow cover using the blue-band classification approach proposed by [16]. It automatically selects a snow threshold based on the blue-band digital number frequency histogram. The method generally delivers robust results but underestimates snow cover in shaded areas [19,28]. Therefore, we additionally applied principal component analysis (PCA), as proposed by [19], to separately classify snow cover in shaded areas. This method, however, overestimates snow cover and classifies bright surfaces such as white rocks as snow if the images contain less than about 50% snow [28]. We therefore applied the PCA method only if the observed area was snow-covered by more than 50% and visually checked the results to avoid error sources caused by snow classification. In addition, we manually labeled small clouds if they disturbed the view on the ground to exclude them from the analysis.

Finally, we created a mask for each webcam to define the area within the webcam image that should be considered for generating the snow-cover maps. Infrastructure, forested areas, and areas that were too far away from the webcams were excluded from the analysis to ensure high quality of the resulting snow cover maps. The snow-classified webcam image was then projected onto a map using the derived transformation matrix. We refer to [28] for more details on the generation of webcam-based snow cover maps.

2.2. Satellite-Based Snow Cover Maps

2.2.1. MODIS Daily Snow Cover Products

We used version 6 of the MODIS data sets MOD10A1 (Terra) and MYD10A1 (Aqua) [34,35]. These data sets have a spatial resolution of 500 m and consist of daily, gridded snow cover information derived from radiance data acquired by MODIS on board the Terra and Aqua satellites. Snow cover information was provided as NDSI, which allows the users to set their own NDSI threshold to optimize the detection of various snow cover conditions [36].

In addition to the two MODIS data sets, we generated a snow cover product by combining the two data sets on a per-pixel basis. If a pixel in the Terra product was cloudy but cloud-free in the Aqua product, the cloudy pixel value was replaced by the NDSI snow cover value of Aqua. This combination strategy is widely used to reduce the cloud cover; see, e.g., [37–41]. It leverages the difference in overpass time between the satellites and the temporal variability in cloud cover to minimize data gaps. According to [14], this method can reduce the cloud coverage ratio by 5%–20% without significantly lowering the product accuracy.

There is an ongoing discussion on the selection of the optimal NDSI threshold to generate binary snow cover maps [26,29,42]. The globally used standard NDSI threshold of 0.4 may be subpar to distinguish snow from snow-free areas [10]. Applying this threshold results in excluding potential snow pixels, since a pixel with NDSI > 0.0 may contain snow cover [10,36]. The optimal NDSI threshold strongly varies in space and time [19] but is typically unknown and difficult to predict for a specific region [42]. In this study, we derived binary snow-cover products using an NDSI of 0.1 and 0.4. From October 2017 to the end of June 2018, six binary snow-cover products (a total of 1638 binary snow cover maps) were generated: MODIS Terra (MOD) NDSI 0.1 and 0.4, MODIS Aqua (MYD) NDSI 0.1 and 0.4, and the combined product (MOYD) NDSI 0.1 and 0.4.

2.2.2. Sentinel-2 Snow Cover Maps

We used the Fractional Snow Cover (FSC) product derived from Sentinel-2A and Sentinel-2B provided by Copernicus Land Monitoring Service (CLMS). Similar to the MODIS snow cover products, the FSC product is based on the ratio of the difference in the visible and shortwave infrared reflectance. It delivers the fraction of the snow covered area at the top of canopy (FSC_{TOC}) and on the ground (FSC_{OG}) and features a spatial resolution of 20 m with a revisit time of five days [11]. The FSC values are based on the Sentinel-2 L1C product. First, an L2A product is generated using the MAJA processor [43], which applies an atmospheric correction, a topographic normalization, and a conservative cloud-masking. Second, binary snow cover maps are generated with the let-it-snow (LIS) processor [9] using a combination of different NDSI thresholds and a digital elevation model. The LIS processor additionally refines the cloud mask by recovering snow pixels from the conservative cloud mask [9]. FSC_{TOC} is calculated from the pixels classified as snow and is based on an empirical relationship that was calibrated using high-resolution satellite data [11]. Finally, FSC_{OG} is derived by incorporating the Tree-Cover Density product delivered by CLMS, which corrects the retrieved snow fraction FSC_{TOG} by accounting for the forest cover [44].

We obtained binary snow cover maps by thresholding $FSC_{OG} > 0$, as suggested by the product user manual [45]. In total, we obtained 37 binary snow cover maps between October 2017 and the end of June 2018.

2.3. Study Area

The 16 webcams are located within the study area of the three hydrological catchments Saane, Sense, and Kander in Switzerland, which cover an area of about 2954 km^2 (see Figure 2). The area covered by the webcam-based snow cover maps is 11.6 km^2, which corresponds to 0.4% of the study area. Due to this small fraction of the study area covered, we selected webcams that were as representative as possible in terms of spatial distribution, altitude, and slope orientation (i.e., evenly distributed over the catchment area). The elevation of the study area ranges from 483 m to 3693 m a.s.l., and the elevation observed by webcams ranges from 715 m to 3128 m a.s.l., with means of 1339 m a.s.l. and 1808 m a.s.l., respectively (see Figure 3). Therefore, elevations below 715 m and above 3128 m were not represented by our webcam data. In addition, the areal coverage observed by webcams was slightly underrepresented around 800 m a.s.l. and between 1000 m and 1800 m a.s.l. The distribution of slope orientation in the whole study area was slightly biased towards the northwest (see Figure 4). The distribution of slope orientation in the area covered by the webcams is further biased towards the northwest: northwestern slopes dominate the area observed by webcams and southern slopes are clearly underrepresented.

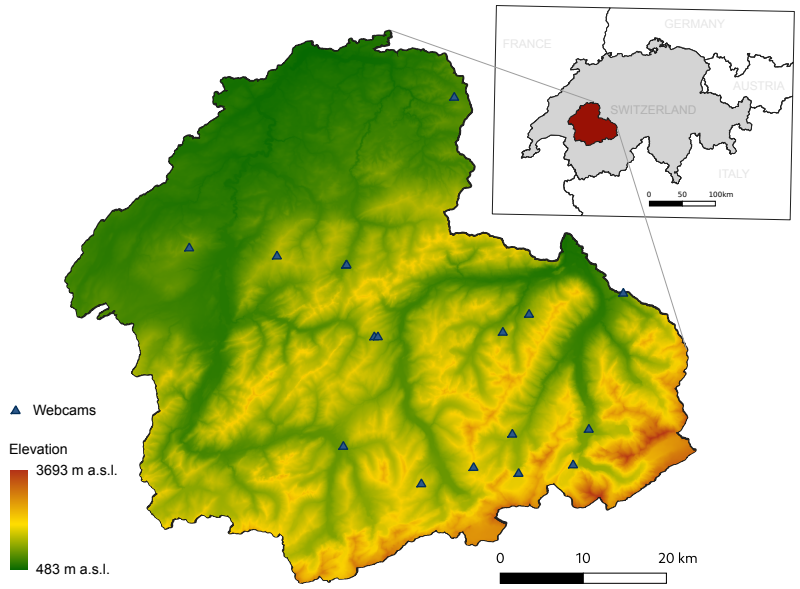

Figure 2. Study area and webcam locations. Background data: swissALTI^{3D} and swissBoundaries © swisstopo.

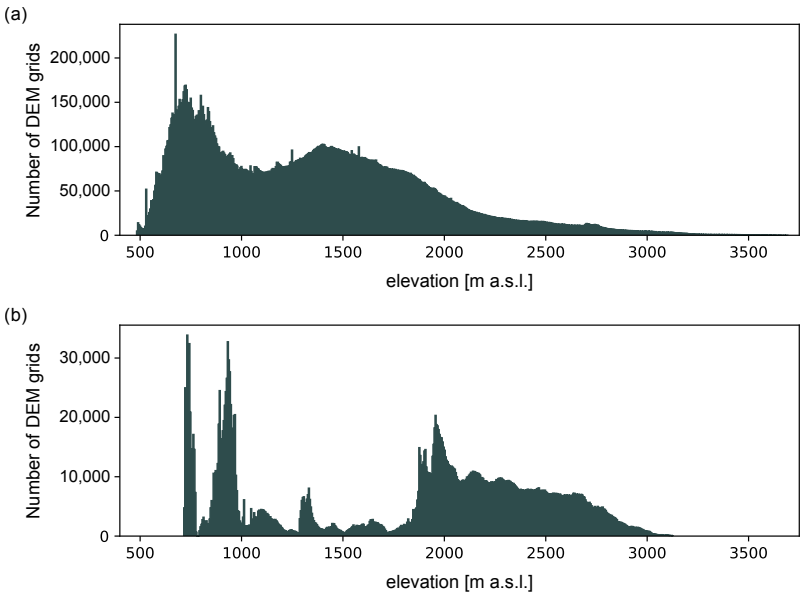

Figure 3. Histogram of the elevation range (**a**) of the whole study area and (**b**) of the area covered by the selected webcams. Note that for (**a**), a 10 m resolution digital elevation model (DEM) and for (**b**), a 2 m resolution DEM was used.

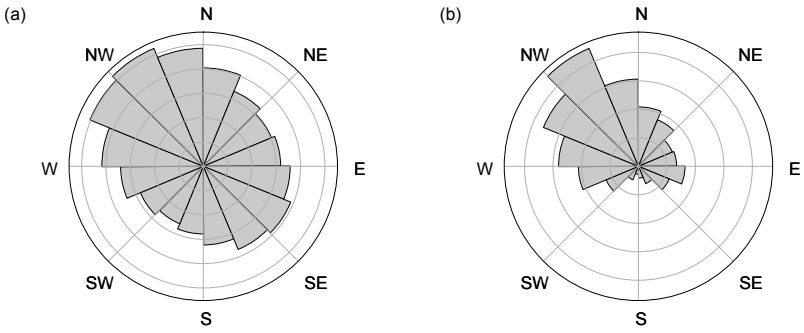

Figure 4. Slope orientation of (**a**) the whole study area and (**b**) the area observed by webcams.

2.4. Regional Snow Line Elevation (RSLE) Estimation

For all data sets considered, we applied the RSLE method proposed by [30]. For each elevation, the sum of snow-free pixels above (P_L) and the sum of snow pixels below (P_S) the respective elevation were computed. The RSLE is defined to be the elevation where the sum of P_L and P_S is minimized. Figure 5 shows an example of the estimated RSLE for a single webcam image in May 2019 and the percentage of $P_S + P_L$ per elevation, normalized by the total number of pixels of the area. The example webcam covers an elevation range between 1103 m a.s.l. and 2762 m a.s.l., and the estimated RSLE is 1743 m a.s.l.

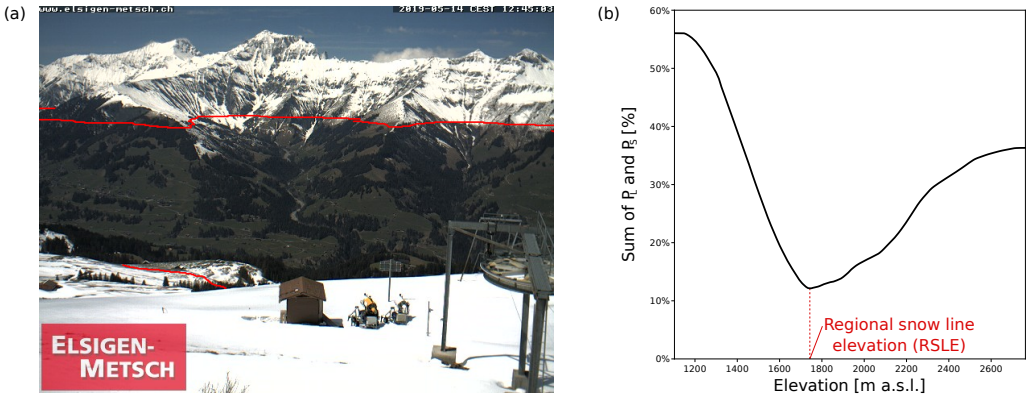

Figure 5. Example of regional snow-line elevation (RSLE) estimation. (**a**) Webcam image from Frutigen Metschalp on 14 May 2019 (© elsigen-metsch.ch (accessed on 24 March 2021)) and estimated RSLE shown in red. (**b**) Percentage of the sum of land pixels above (P_L) and snow-covered pixels below (P_S) each elevation with respect to the total number of pixels. The estimated RSLE is the elevation where the sum of P_L and P_S is minimized (1743 m a.s.l.).

We used the swissALTI^{3D} DEM with a spatial resolution of 2 m [31] to derive RSLE estimates using the webcam data set. The same DEM, downsampled to 10 m resolution, was used to derive RSLE estimates from the Sentinel-2 snow cover maps. For the RSLE retrieval of the MODIS snow cover maps, we used the DEM DHM25 with a grid size of 25 m provided by the Swiss Federal Office of Topography [46].

The RSLE estimation method was applied to all MODIS and Sentinel-2 scenes with a cloud coverage of less than 70%. In addition, we used only those MODIS snow cover maps that had a minimum snow coverage of 5%. These thresholds were selected based on a sensitivity analysis carried out by [30] by examining the impact of cloud and minimum snow cover thresholds on the accuracy and data availability of RSLE estimation using MODIS data in Slovakia. The reason for applying the 5% snow threshold is that RSLE estimation requires enough snow pixels to work robustly. Such a snow threshold is not required in the case of Sentinel-2, since the higher spatial resolution yields a sufficient number of snow pixels, unlike MODIS.

3. Results

3.1. Impact of Cloud Cover on Temporal Resolution

The percentage of daily webcam images covered by clouds varies across different webcams (see Figure 6). In general, webcams observing smaller areas close to the camera are least affected by cloud coverage. If the observed area spans less than 76,000 m^2 (which holds for half of the selected webcams), less than 4% of the daily webcam images contain some cloud cover. On the other hand, the webcam Adelboden Chefihuesi, which observes an area of 2.3 km^2, is affected by cloud cover in 26% of the daily images.

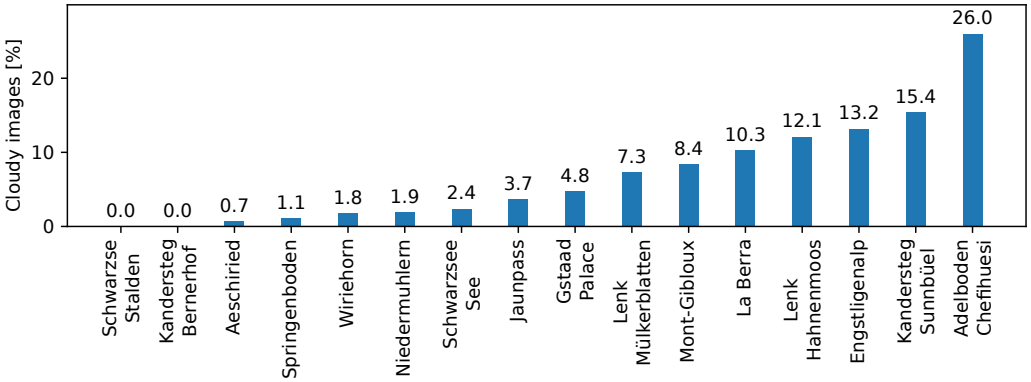

Figure 6. Percentage of cloudy images of the selected webcams during the investigated time period between October 2017 and end of June 2018.

As mentioned in Section 2.1, an average of 14.3 webcam images per day were available. On average, 0.4 images were fully cloud covered, and 0.7 images were partly cloud covered. Since we manually labeled images with partial cloud coverage, we were able to use an average of 13.9 webcam images per day to estimate the RSLE. On six days, at most 10 images were available. Whether a decreased number of webcams affects the accuracy of the RSLE estimate depends on the observed elevation range of the cloud-covered webcams in relation to the elevation of the true snow line. Over the entire investigation period between October 2017 and the end of June 2018, cloud cover led to a data gap of a single day: on 13 June 2018, we were not able to estimate the RSLE since cloud-free webcam information was only available below 1717 m a.s.l.

During the investigation period, the MOD and MYD snow cover maps had a mean cloud coverage of 65.9% and 69.4%, respectively. Merging MOD and MYD (MOYD) reduces the mean cloud coverage to 60.1%. The Sentinel-2 snow cover product has a mean cloud coverage of 50.0%. However, FSC maps with a cloud coverage of more than 90% were discarded and thus were not available for download. Therefore, the actual mean cloud coverage of the Sentinel-2 snow cover maps is higher.

Table 1 shows the number of available snow-cover maps of MODIS and Sentinel-2 and how this number was lowered by applying different cloud thresholds and the snow threshold of 5%. By applying a cloud-cover threshold of 70%, 56.2% (MOD) and 59.7% (MYD) of the scenes were discarded, resulting in 120 and 110 available scenes for MOD and MYD, respectively. Using the merged snow-cover product MOYD increased the number of available scenes to 139. However, about 15% (MOD, MOYD) and 16% (MYD) of all scenes contained less than 5% of snow pixels, resulting in 79 (MOD), 66 (MYD), and 97 (MOYD) scenes remaining for the actual RSLE estimation. Applying a cloud threshold of 70% to the Sentinel-2 snow cover maps reduced the 37 maps to 27 snow-cover maps.

Table 1. Number of available snow-cover maps and the impact of the selected cloud threshold on data availability of MODIS and Sentinel-2 snow-cover maps. For the MODIS data sets, the snow threshold of 5% was applied additionally, whereas for the Sentinel-2 snow-cover data set, only cloud thresholds were applied to calculate the number of scenes.

Cloud Threshold	100%	90%	80%	70%	60%
MOD	104	97	86	79	69
MYD	87	79	74	66	58
MOYD	123	112	102	97	86
Sentinel-2	37	33	30	27	23

Figure 7 shows the number and length of the data gaps in the MODIS and Sentinel-2 snow-cover products using a cloud-cover threshold of 70%. The resulting data gaps last up to 11 days in the MOD, MYD, and MOYD snow-cover products. These data gaps do

not include gaps caused by applying the 5% snow threshold, which mainly affects snow cover maps before 20 October 2017, and most of the snow cover maps in May and June 2018. For Sentinel-2, seven data gaps between 15 and 55 days occurred between October 2017 and end of June 2018 when a cloud threshold of 70% was applied.

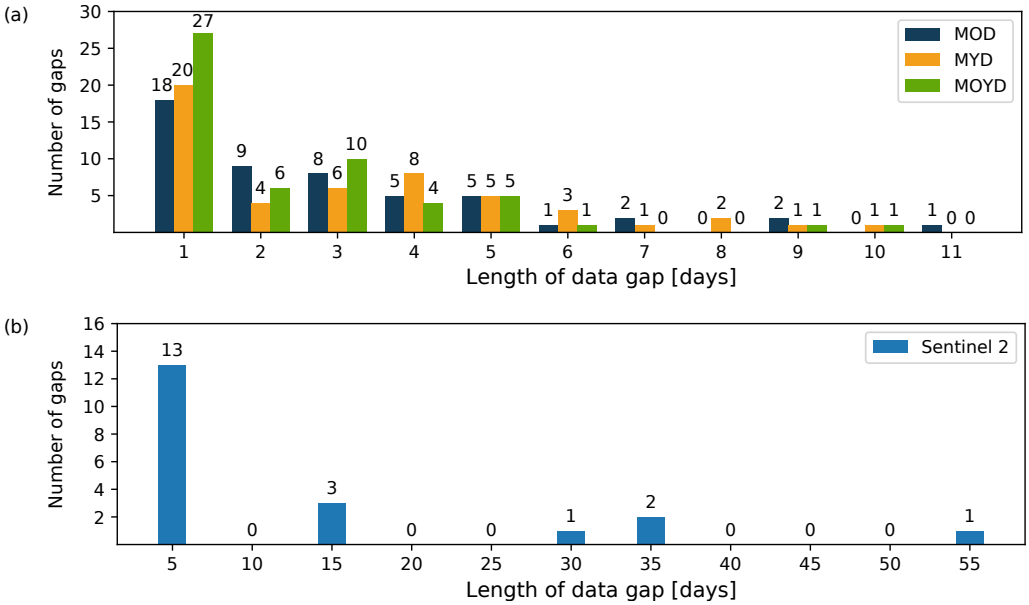

Figure 7. Length of data gaps in the (**a**) MOD, MYD, MOYD, and (**b**) Sentinel-2 data sets caused by using a cloud cover threshold of 70%.

Figure 8 shows the moving average (window size of 30 days) of the percentage of available MOYD snow-cover maps. In addition, data gaps are shaded in blue. In February and March, rather short data gaps of up to six days occurred frequently, reducing the number of available scenes significantly.

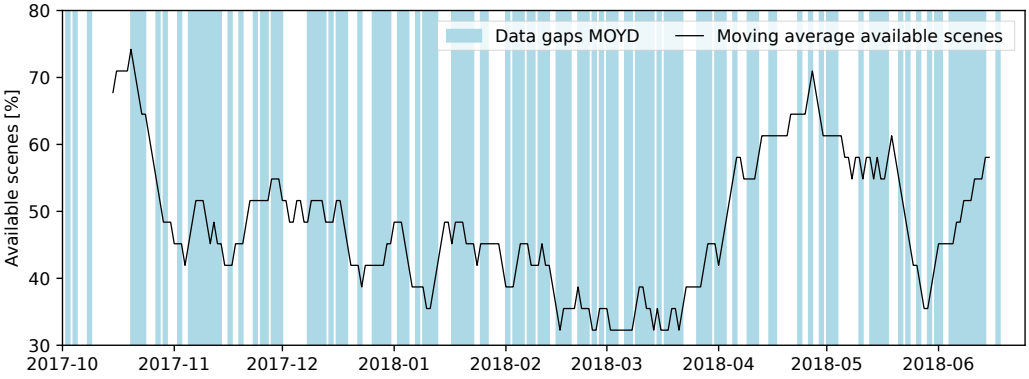

Figure 8. Data gaps of MOYD (blue) and moving average (window size of 30 days) of the percentage of available MOYD snow cover maps.

3.2. Regional Snow Line Elevation (RSLE)

In Figure 9, we compare the webcam RSLE with the RSLE derived from MOYD and Sentinel-2 snow-cover data. The RSLE derived from webcam measurements highlights the ability of the webcam measurements to capture the high variability in the RSLE within the investigated time period. Overall, the derived RSLE trend agrees well with the satellite-based measurements. The time series can be divided into three main periods: (1) a decreasing RSLE between October and end of November, (2) a period with relatively low RSLE between December and March, and (3) an increasing RSLE from March until the end of June (see Figure 9a).

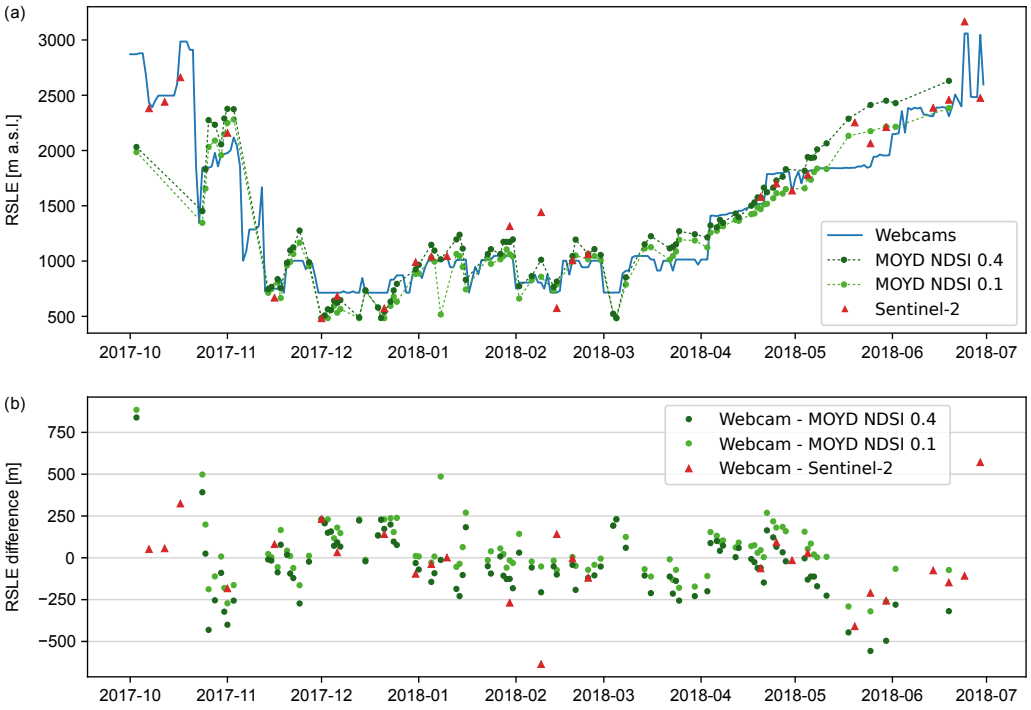

Figure 9. (**a**) Regional snow line elevation (RSLE) derived from webcams, MOYD, and Sentinel-2 snow-cover data sets and (**b**) differences between webcam RSLEs and MOYD/Sentinel-2 RSLEs.

In period (1), there is an overall decrease in webcam RSLE from about 3000 m to 714 m a.s.l. The main difference between webcam- and satellite-based estimates is that the webcams capture events between consecutive satellite-based measurements, whereas measurements from satellites feature large temporal gaps, e.g., during the first two weeks of November. In addition, the RSLE estimated from webcam measurements is often significantly lower than that of satellite-based estimates, for instance, in the period between the end of October and the beginning of November.

During the low-RSLE period (2), the estimated webcam RSLEs vary between 714 m a.s.l. and 1072 m a.s.l. The most salient differences between webcam- and satellite-based estimates appear largely inverted compared to the differences in period (1); i.e., the RSLE derived from webcams is often significantly above the satellite-based estimate (e.g., in December and beginning of March). In addition, high-RSLE periods (e.g., in January) show lower estimates from webcam-based measurements compared to satellite data, which is similar to the discrepancy observed during period (1).

Finally, period (3) shows a relatively continuous RSLE increase from about 715 m a.s.l. in March to 2500–3000 m a.s.l. at the end of June. The most apparent difference in satellite- and webcam-based estimates is that while the former shows a smooth and almost constant increase, webcam-based measurements result in a more stepwise pattern, causing large discrepancies where the webcam-based RSLE is below the one derived from satellite data and small discrepancies where the difference is opposite.

Analysis of RSLE Differences between Webcam- and Satellite-Based Estimates

Table 2 shows mean values and standard deviations of the differences between RSLEs estimated from webcams and reference data sets. Overall, webcam RSLEs are most similar to the retrieval from MODIS with an NDSI of 0.1 (mean differences of 44.7 m (MOD), 22.7 m (MYD), and 31.4 m (MOYD)). Using this NDSI setting, 60.1% of all MODIS RSLE estimates are below webcam RSLE estimates. Increasing the NDSI to 0.4 causes 70.4% of all MODIS RSLE estimates to be higher than the webcam estimates, with mean differences between 47 m (MOD) and 73.7 m (MOYD). The comparison with Sentinel-2 RSLEs reveals a mean RSLE difference of 53.1 m and a remarkably large standard deviation.

Table 2. Mean and standard deviation of differences between webcam regional snow line elevation (RSLE) and MODIS/Sentinel-2 RSLE.

		Mean	σ
Webcam−MOD	NDSI 0.1	44.69	127.45
	NDSI 0.4	−47.46	147.68
Webcam−MYD	NDSI 0.1	22.66	130.71
	NDSI 0.4	−64.16	138.48
Webcam−MOYD	NDSI 0.1	31.41	172.28
	NDSI 0.4	−73.65	189.11
Webcam−Sentinel-2		−53.13	229.24

To qualitatively analyze RSLE differences between satellite- and webcam-based estimates, we consider images of webcams that observe the elevation range around the estimated RSLEs. Our analysis reveals the following main reasons for the observed discrepancies: *clipping*, *data gaps*, *misclassification*, *slope exposure*, and *daytime*. In the following paragraphs, we discuss these reasons in detail.

Clipping: If the actual RSLE lies below the lower bound of the webcam-observed elevation range (714 m a.s.l. in our area of investigation), the webcam-based approach overestimates the RSLE, making an accurate RSLE derivation impossible. An example of this condition is the period in December, when snow fell down deep into the Swiss lowlands. Such conditions occur solely during low-RSLE periods, indicating the need to include more low-elevation webcams to measure RSLE during winter months. In our analysis (i.e., Table 2), we exclude data points if the estimated webcam RSLE is below <720 m a.s.l., which applies for 33 days.

Data gaps: Significant cloud coverage that hinders the view on the surface results in temporal gaps in satellite-based measurements, whereas webcams are often unaffected due to being located below or above the cloud cover. An example of this situation is the time period between October and November, where five major decreases in RSLE are estimated by the webcam-based approach. The weekly winter reports provided by the Institute for Snow and Avalanche Research (SLF) part of the The Swiss Federal Institute for Forest Snow and Landscape Research (WSL) confirm the exact dates of the respective decreases in RSLE (October 6, 22 to 23; November 6, 13, and 28 to 30) [47,48]. These drops are caused by major precipitation events paired with significant decreases in temperature. The satellite-based RSLE estimates do not capture parts of these dynamics due to data gaps caused by cloud cover, which naturally co-occur with precipitation events.

Misclassification: Snow maps derived from satellite-based measurements frequently misclassify snow cover due to a high amount of cloud cover and resulting snow/cloud discrimination errors. One such example can be observed on October 3, where the discrepancy in RSLE between MOYD and the webcam is more than 750 m (see Figure 9b). Considering the snow maps derived from both MOD and MYD, we observe that both products misclassify clouds as snow. Moreover, the zero-degree line as well as the snowfall level were reported to be above 3000 m a.s.l. at that day [47]. Overall, MOYD clearly underestimates the RSLE under such conditions. Another example is February 14, when the Sentinel-2 snow cover map contains cloud cover that disturbs the view on the lowlands. Only a few land pixels are visible, which leads to an underestimation of the RSLE. Another source of misclassification is the occurrence of shadows cast by surrounding mountains, causing dark snow pixels to be misclassified as land pixels. This situation is most severe during periods of low solar altitude. On February 9, for instance, the Sentinel-2 snow cover map contains major areas of missing snow cover caused by such shadows. The resulting RSLE estimate clearly differs from RSLEs estimated by the MOYD and webcam measurements.

Slope exposure: In Section 2.3, we identified a strong bias towards north-facing slopes in the area observed by our webcams. This bias is the main reason our webcam-based

approach frequently estimates a lower RSLE than the satellite-based counterparts. We observe the largest differences around May. During this period, the webcam-based RSLE estimates are around 1900 m a.s.l. In this elevation range, three out of four of our webcams (Kandersteg Sunnbüel, Lenk Mülkerblatten, and Lenk Hahnenmoos) mainly monitored north-facing slopes. Figure 10 shows two webcam images captured on 18 May 2018. In both examples, we mark the RSLEs estimated by webcams (red line) and MOYD (orange and green lines). The webcam Frutigen Metschalp (Figure 10a, not included in our study) observes mostly northern, southern, and eastern slopes. The webcam-based approach underestimates the RSLE in this area. In contrast, the webcam Kandersteg Sunnbüel (Figure 10b) mainly observes the snow cover at a north-northwestern slope, where snow remains longer compared to snow on south-facing slopes that is exposed to more direct solar illumination. In this example, MOYD overestimates the RSLE.

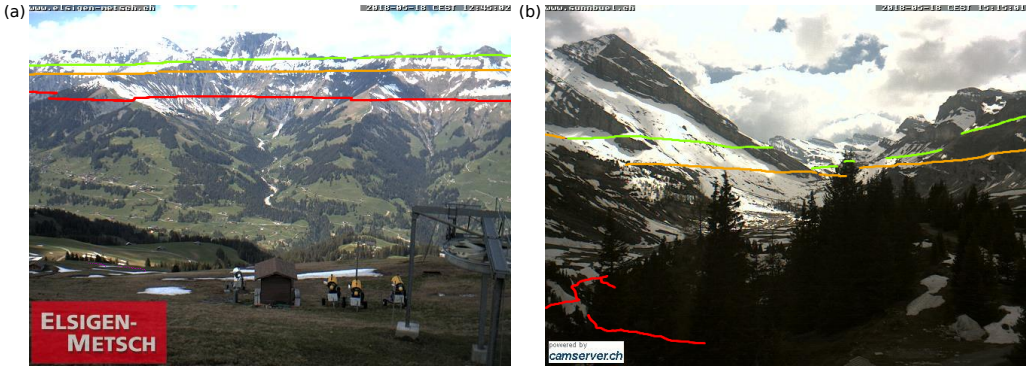

Figure 10. Differences in regional snow-line elevation (RSLE) shown on images of the webcams (**a**) Frutigen Metschalp (© elsigen-metsch.ch (accessed on 24 March 2021)) and (**b**) Kandersteg Sunnbüel (© www.sunnbuel.ch (accessed on 24 March 2021)). RSLE is marked in red (webcams), orange (MOYD product with NDSI 0.1), and green (MOYD product with NDSI 0.4).

Daytime: We have identified some differences in RSLE caused by the sub-daily variability in the actual RSLE and the fact that the data sets were captured at different times of day. In general, sub-daily variability in RSLE is assumed to be small. As an example, the mean RSLE difference between MOD and MYD (about 3h difference in overpass time) was 23 m (NDSI 0.1) and 17.6 m (NDSI 0.4) during the investigated time period. However, abrupt weather changes such as heavy precipitation events or significant changes in temperature may lead to major changes in RSLE over a short period. A high sub-daily variability in RSLE was observed on October 24, for example (see Figure 11). When hourly webcam images were used, the calculated RSLE shows an increase from 1450 m a.s.l. to 2098 m a.s.l. between 7:45 and 18:45 local time (UTC+2). This RSLE increase of almost 650 m can explain some of the difference between the daily webcam RSLE and MOYD RSLE. On October 24, many of the selected webcam images were observing mountain ranges in the late afternoon, resulting in an RSLE estimated at 1844 m a.s.l. MOYD RSLE is estimated at 1346 m a.s.l. (NDSI 0.1) and 1452 m a.s.l. (NDSI 0.4), which, however, seems to underestimate the actual RSLE of the whole day for the scene shown in Figure 12. Figure 12 shows two webcam images on October 24 at 8:00 and 17:00 local time (UTC+2) and estimates of MOYD RSLE and corresponding hourly webcam RSLE estimates. Nevertheless, the increased difference between MOD and MYD (171 m and 146 m using an NDSI 0.1 and 0.4, respectively) depicts the high sub-daily variability on that day as well.

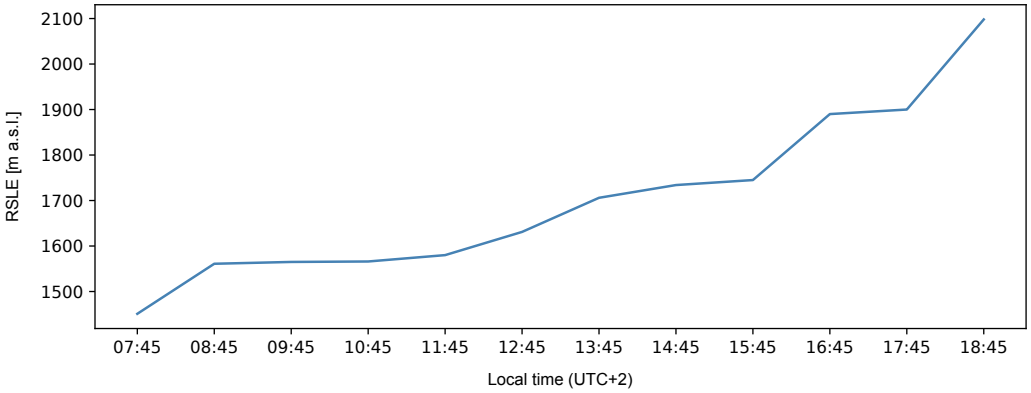

Figure 11. Daytime variability of the regional snow line elevation (RSLE) on 24 October 2017. The RSLE values were estimated using hourly webcam images.

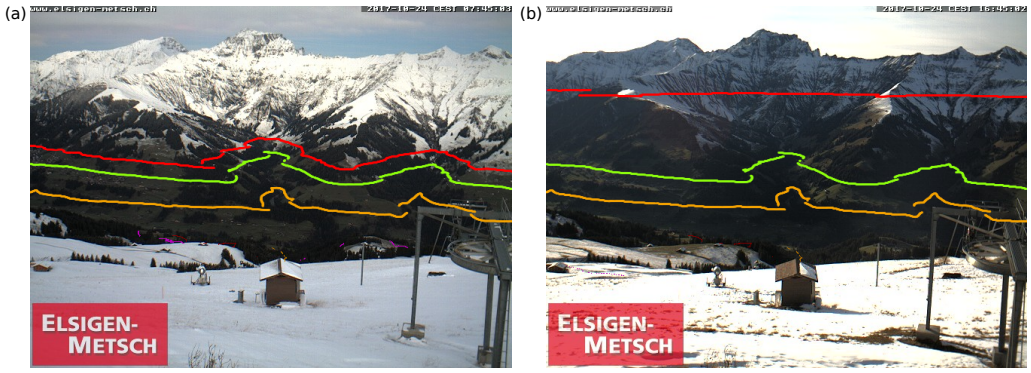

Figure 12. Regional snow line elevation (RSLE) differences on 24 October 2017 at (**a**) 7:45 and (**b**) 16:45 local time (UTC+2) between hourly webcam RSLE (red line) and MOYD RSLE using an NDSI of 0.1 (orange line) and 0.4 (green line). Webcam image: Frutigen Metschalp (© elsigen-metsch.ch (accessed on 24 March 2021)).

4. Discussion

In the investigated time period, data availability of optical satellite data is highly affected by cloud coverage. The mean cloud coverage of more than 60% observed for MODIS data is in line with the study by Parajka et al. [49], which reports an average cloud coverage of 63% between 2000 and 2005 in Austria. Applying a cloud threshold of 70% to estimate RSLE therefore significantly reduces the number of available scenes in the investigated time period. While raising this threshold would increase the number of available measurements, it would decrease the accuracy of the RSLE estimation, resulting in a tradeoff that cannot be resolved in a straightforward manner [30]. We observe that cloud cover affects the number of available scenes, particularly during February and March, whereas April and May are less affected. However, a recent study by Parajka et al. [50] reports mean cloud coverage of more than 80% during runoff peaks in different alpine catchment areas. Therefore, webcams can provide a valuable contribution to enhance the knowledge of snow-water resources during melting periods in particular, especially when hourly webcam data are available.

Using 16 public webcams, we managed to build a continuous snow-line time-series covering 273 days. By leveraging our hourly webcam data archive, the impact of cloud cover on snow-line retrieval is minimized, resulting in only one day of missing data due to excessive cloud coverage. Note that the effect of cloud cover depends on the webcam location. While webcams that observe areas at large distances of several kilometers cover both the large elevation range and area, such measurements are more often affected by clouds, disturbing the view on the ground. We therefore recommend combining such measurements with webcams that observe small areas (i.e., less than about 50,000 m^2), since the probability that clouds disturb the view on the ground during an entire day decreases

with reduced observation distance. To further mitigate the effects of cloud cover, more than one webcam should observe the same elevation range to leverage the spatial variability of cloud cover.

The comparison of webcam-based RSLE with snow-line retrieval from satellite data shows that webcams can represent regional snow lines of a large area with only a few webcams. Our analysis shows that the largest differences between webcam- and satellite-based RSLE can be attributed to classification errors in MODIS and Sentinel-2 snow cover maps, the impact of north-facing slopes on webcam RSLE, the clipped observation elevation for the selected webcams, and the daily variability in RSLE. However, other influences must be considered as well, such as the impact of forested areas. In our webcam data set, forested areas were excluded explicitly for snow-line estimation, whereas MODIS and Sentinel-2 data sets cover the entire study area. While FSC maps of Sentinel-2 do incorporate a tree-cover density correction, this correction does not affect our binary snow cover maps, since we set all FSC vaues > 0.1 to snow (see Section 2.2.2). Note that including forested areas in the webcam data set would mostly increase webcam-based RSLE elevations and therefore decrease RSLE differences between webcam, MODIS (NDSI 0.4), and Sentinel-2 data sets. Another hyperparameter that causes RSLE differences between webcam- and satellite-based estimations is the choice of the NDSI threshold for satellite-based snow classification, which directly determines the RSLE estimation. As mentioned in Section 2.2.1, there is ongoing discussion on the selection of the optimal NDSI threshold. In the Sentinel-2 snow-cover product, snow is first detected using an NDSI of 0.4 in order to minimize false snow detection. Next, the minimum snow elevation is determined, above which the snow detection is further refined using an NDSI of 0.15 [9]. Under the assumption that applying an NDSI of 0.4 underestimates the snow-covered area, this approach leads to an overestimate of Sentinel-2-based RSLE, which decreases the discrepancy between our webcam-based estimation and Sentinel-2 estimation further. Finally, it must be considered that satellite-based snow cover mapping is constantly improved and new methodologies based on extended spectral characteristics or deep learning have been developed, e.g., [51,52]. It would be worthwhile investigating webcam RSLE differences with such products in the future.

Overall, the high temporal resolution and the possibility of observing snow conditions below cloud coverage are the main advantages of the webcam-based approach for RSLE estimation. The registration approach proposed by Portenier et al. [28] enables the mapping of pixel information from webcam images with minimal amount of manual user input. An evaluation of this approach using ground control points reveals a root mean square error of 23.7 m [28]. This accuracy is sufficient to augment satellite-based snow cover retrieval, given that the spatial resolution is typically lower. However, the mapping could be improved further by leveraging more accurate camera models or manual georeferencing tools. With regard to the enormous number of available webcam data, we recommend further improving and automating the processing of webcam data. In particular, there is significant room for improvement in the performance of current snow-classification techniques on RGB images to avoid a manual verification and correction. The study of Salvatori et al. [16] reports 2–3% of snow-covered pixels not detected by their blue-band classification approach due to snow cover in shaded areas if a 100%-snow-covered image is considered. The study by Härer et al. [19] reports that the PCA approach was successfully applied in at least 95% of their shadow-affected images. However, the performance of both methods highly depends on the webcam images and its illumination conditions. We think that the performance of snow classification could be greatly improved by leveraging deep learning techniques. It has already been proven that supervised learning classifiers such as Random Forest outperform threshold-based approaches such as the blue-band classification [22]. Likewise, methods for automatic cloud detection would considerably simplify the process of webcam-based snow-cover retrieval, which would enable even larger-scale studies. Even though such methods require a large number of ground truth labeled data for training, we consider this a promising direction for future work. One of the main issues with using public webcam data is their data availability. To the best

of our knowledge, no large-scale, publicly accessible webcam archives exist. Therefore, measured data must be stored instantly and continuously, rendering retrospective changes to the webcam selection and sampling interval infeasible. As a consequence, the data collection protocol must be designed carefully and implemented rigorously to avoid biases towards particular impacts such as slope orientation, elevation, or spatial distribution. Moreover, long time series can only be achieved by maintaining the data collection pipeline throughout the entire investigation period. However, with ensured data access, webcam-based snow-cover mapping offers a huge potential to observe large-scale catchment areas and to complement satellite-based snow-cover mapping.

5. Conclusions

In the present study, we derived the regional snow-line elevation in an alpine catchment area using 16 public webcams. The webcam-based estimation enables the high dynamics of the snow line to be depicted thanks to its nearly continuous measurements. In addition, the ability to fill gaps in satellite-based snow cover information caused by cloud coverage shows great potential in complementing and improving such data. We investigated the differences between snow line estimates derived from webcams and different satellite-based products from MODIS and Sentinel-2, and we have illustrated that webcams can represent regional snow line elevations of a large area using only a few webcams. The resulting mean differences from satellite-based techniques (22.66–73.65 m, depending on the choice of the satellite-based product) indicate great agreement, and we identified different melting rates at north- and south-facing slopes as the main reason for the observed differences. In addition, we have shown that sub-daily snow line variability, classification errors in MODIS and Sentinel-2 snow cover maps, and a clipped observation elevation due to the selection of webcam locations cause additional differences.

Not only is webcam-based snow cover information a powerful data source to complement and thereby improve satellite-based RSLE retrieval, but we found that webcam images are a valuable source of information to qualitatively evaluate and visualize differences in snow lines estimated by different approaches as well. While several studies have already shown that daily snow cover information from webcams can be used to validate satellite-based snow cover retrieval, we think that it can also serve to improve the hydrological modeling of available water resources, especially during melting periods with increased cloud cover, where satellite-based approaches suffer from data gaps. Moreover, a large webcam network with local snow information and a high temporal resolution could not only be used to study snow metamorphism or observe avalanche risks but can also be used to improve snow classification by correlating snow pixels observed by webcams with satellite-based observations. In the future, we will investigate improvements in snow classification and the potential of deep learning techniques for automatic cloud detection in webcam images. In addition, evaluating and complementing traditional gap-filling methods by means of webcam data would be worth investigating. For instance, the accuracy of the recent daily cloud-free MODIS snow cover data sets MOD10A1F and MYD10A1F provided by the NASA Distributed Active Archive Center at NSIDC could be quantified using ground truth measurements from webcams. Similarly, the incorporation of webcam-based measurements to improve gap-filling techniques for satellite data is a promising direction for future work. Given the availability of an appropriate archive of webcams, webcam-derived snow-cover information could greatly enhance their performance.

Author Contributions: Conceptualization, C.P. and S.W.; methodology and software, C.P.; formal analysis, C.P. and M.H.; writing—original draft preparation, C.P.; writing—review and editing, C.P. and S.W.; supervision, S.W. All authors have read and agreed to the published version of the manuscript.

Funding: This research received no external funding.

Data Availability Statement: The webcam data are available on request from the corresponding author and are not publicly available due to copyright protection. The webcam-based snow cover data are available at https://bit.ly/3OwFy6O (accessed on 28 June 2022). The Sentinel-2 and MODIS snow cover data sets are openly available in [44,45] and [34,35], respectively.

Acknowledgments: We kindly acknowledge Kai Kobler for providing webcam images on www.kaikowetter.ch (accessed on 28 June 2022) and sincerely thank all the webcam owners that share their images online.

Conflicts of Interest: The authors declare no conflict of interest.

References

1. Déry, S.J.; Brown, R.D. Recent Northern Hemisphere snow cover extent trends and implications for the snow-albedo feedback. *Geophys. Res. Lett.* **2007**, *34*. [CrossRef]
2. Barnett, T.P.; Adam, J.C.; Lettenmaier, D.P. Potential impacts of a warming climate on water availability in snow-dominated regions. *Nature* **2005**, *438*, 303–309. [CrossRef] [PubMed]
3. Jonas, T.; Rixen, C.; Sturm, M.; Stoeckli, V. How alpine plant growth is linked to snow cover and climate variability. *J. Geophys. Res. Biogeosci.* **2008**, *113*. [CrossRef]
4. Wipf, S.; Rixen, C. A review of snow manipulation experiments in Arctic and alpine tundra ecosystems. *Polar Res.* **2010**, *29*, 95–109. [CrossRef]
5. Rixen, C.; Teich, M.; Lardelli, C.; Gallati, D.; Pohl, M.; Ptz, M.; Bebi, P. Winter tourism and climate change in the Alps: An assessment of resource consumption, snow reliability, and future snowmaking potential. *Mt. Res. Dev.* **2011**, *31*, 229–236. [CrossRef]
6. Dietz, A.J.; Wohner, C.; Kuenzer, C. European snow cover characteristics between 2000 and 2011 derived from improved MODIS daily snow cover products. *Remote Sens.* **2012**, *4*, 2432–2454. [CrossRef]
7. Hüsler, F.; Jonas, T.; Riffler, M.; Musial, J.P.; Wunderle, S. A satellite-based snow cover climatology (1985–2011) for the European Alps derived from AVHRR data. *Cryosphere* **2014**, *8*, 73–90. [CrossRef]
8. Gascoin, S.; Hagolle, O.; Huc, M.; Jarlan, L.; Dejoux, J.F.; Szczypta, C.; Marti, R.; Sánchez, R. A snow cover climatology for the Pyrenees from MODIS snow products. *Hydrol. Earth Syst. Sci.* **2015**, *19*, 2337–2351. [CrossRef]
9. Gascoin, S.; Grizonnet, M.; Bouchet, M.; Salgues, G.; Hagolle, O. Theia Snow collection: High-resolution operational snow cover maps from Sentinel-2 and Landsat-8 data. *Earth Syst. Sci. Data* **2019**, *11*, 493–514. [CrossRef]
10. Riggs, G.A.; Hall, D.K.; Román, M.O. Overview of NASA's MODIS and Visible Infrared Imaging Radiometer Suite (VIIRS) snow-cover Earth System Data Records. *Earth Syst. Sci. Data* **2017**, *9*, 765–777. [CrossRef]
11. Gascoin, S.; Dumont, Z.B.; Deschamps-Berger, C.; Marti, F.; Salgues, G.; López-Moreno, J.I.; Revuelto, J.; Michon, T.; Schattan, P.; Hagolle, O. Estimating fractional snow cover in open terrain from Sentinel-2 using the normalized difference snow index. *Remote Sens.* **2020**, *12*, 2904. [CrossRef]
12. Parajka, J.; Pepe, M.; Rampini, A.; Rossi, S.; Blöschl, G. A regional snow-line method for estimating snow cover from MODIS during cloud cover. *J. Hydrol.* **2010**, *381*, 203–212. [CrossRef]
13. Hall, D.; Riggs, G.; DiGirolamo, N.; Román, M. MODIS Cloud-Gap Filled Snow-Cover Products: Advantages and Uncertainties. *Hydrol. Earth Syst. Sci. Discuss.* **2019**, 1–23. [CrossRef]
14. Li, X.; Jing, Y.; Shen, H.; Zhang, L. The recent developments in cloud removal approaches of MODIS snow cover product. *Hydrol. Earth Syst. Sci.* **2019**, *23*, 2401–2416. [CrossRef]
15. Farinotti, D.; Magnusson, J.; Huss, M.; Bauder, A. Snow accumulation distribution inferred from time-lapse photography and simple modelling. *Hydrol. Process.* **2010**, *24*, 2087–2097. [CrossRef]
16. Salvatori, R.; Plini, P.; Giusto, M.; Valt, M.; Salzano, R.; Montagnoli, M.; Cagnati, A.; Crepaz, G.; Sigismondi, D. Snow cover monitoring with images from digital camera systems. *Ital. J. Remote Sens./Riv. Ital. Di Telerilevamento* **2011**, *43*, 137–145. [CrossRef]
17. Parajka, J.; Haas, P.; Kirnbauer, R.; Jansa, J.; Blöschl, G. Potential of time-lapse photography of snow for hydrological purposes at the small catchment scale. *Hydrol. Process.* **2012**, *26*, 3327–3337. [CrossRef]
18. Härer, S.; Bernhardt, M.; Corripio, J.G.; Schulz, K. PRACTISE – Photo Rectification Furthermore, ClassificaTIon SoftwarE (V.1.0). *Geosci. Model Dev.* **2013**, *6*, 837–848. [CrossRef]
19. Härer, S.; Bernhardt, M.; Schulz, K. PRACTISE – Photo Rectification Furthermore, ClassificaTIon SoftwarE (V.2.1). *Geosci. Model Dev.* **2016**, *9*, 307–321. [CrossRef]
20. Pimentel, R.; Pérez-Palazón, M.J.; Herrero, J.; Polo, M.J. Monitoring Snow Cover Area In Semiarid Regions Using Terrestrial Photography. In Proceedings of the 11th International Conference on Hydroinformatics, HIC 2014, New York, NY, USA, 17–21 August 2014; p. 378.
21. Liu, J.-f.; Chen, R.-s.; Wang, G. Snowline and snow cover monitoring at high spatial resolution in a mountainous river basin based on a time-lapse camera at a daily scale. *J. Mt. Sci.* **2015**, *12*, 60–69. [CrossRef]
22. Fedorov, R.; Camerada, A.; Fraternali, P.; Tagliasacchi, M. Estimating Snow Cover from Publicly Available Images. *IEEE Trans. Multimed.* **2016**, *18*, 1187–1200. [CrossRef]

23. Millet, P.; Huwald, H.; Weijs, S.V. Extracting High Resolution Snow Distribution Information with Inexpensive Autonomous Cameras. In Proceedings of the HIC 2018—13th International Conference on Hydroinformatics, Palermo, Italy, 1–6 July 2018; EPiC Series in Engineering; Loggia, G.L., Freni, G., Puleo, V., Marchis, M.D., Eds.; EasyChair: Manchester, UK, 2018; Volume 3, pp. 1397–1405. [CrossRef]
24. Flöry, S.; Ressl, C.; Hollaus, M.; Pürcher, G.; Piermattei, L.; Pfeifer, N. WEBSNOW: ESTIMATION of snow cover from freely accessible webcam images in the alps. *ISPRS Ann. Photogramm. Remote Sens. Spatial Inf. Sci.* **2020**, *5*, 695–701. [CrossRef]
25. Piazzi, G.; Tanis, C.M.; Kuter, S.; Simsek, B.; Puca, S.; Toniazzo, A.; Takala, M.; Akyürek, Z.; Gabellani, S.; Arslan, A.N. Cross-country assessment of H-SAF snow products by sentinel-2 imagery validated against in situ observations and webcam photography. *Geosciences* **2019**, *9*, 129. [CrossRef]
26. Aalstad, K.; Westermann, S.; Bertino, L. Evaluating satellite retrieved fractional snow-covered area at a high-Arctic site using terrestrial photography. *Remote Sens. Environ.* **2020**, *239*, 111618. [CrossRef]
27. Hu, Z.; Dietz, A.; Kuenzer, C. The potential of retrieving snow line dynamics from Landsat during the end of the ablation seasons between 1982 and 2017 in European mountains. *Int. J. Appl. Earth Obs. Geoinf.* **2019**, *78*, 138–148. [CrossRef]
28. Portenier, C.; Hüsler, F.; Härer, S.; Wunderle, S. Towards a webcam-based snow cover monitoring network: Methodology and evaluation. *Cryosphere* **2020**, *14*, 1409–1423. [CrossRef]
29. Härer, S.; Bernhardt, M.; Siebers, M.; Schulz, K. On the need for a time- and location-dependent estimation of the NDSI threshold value for reducing existing uncertainties in snow cover maps at different scales. *Cryosphere* **2018**, *12*, 1629–1642. [CrossRef]
30. Krajčí, P.; Holko, L.; Perdigão, R.A.; Parajka, J. Estimation of regional snowline elevation (RSLE) from MODIS images for seasonally snow covered mountain basins. *J. Hydrol.* **2014**, *519*, 1769–1778. [CrossRef]
31. Federal Office of Topography Swisstopo. swissALTI3D, the hIgh Precision Digital Elevation Model of Switzerland. Available online: https://www.swisstopo.admin.ch/en/geodata/height/alti3d.html (accessed on 15 March 2021).
32. Lowe, D.G. Distinctive Image Features from Scale-Invariant Keypoints. *Int. J. Comput. Vis.* **2004**, *60*, 91–110. [CrossRef]
33. Fischler, M.A.; Bolles, R.C. Random Sample Consensus: A Paradigm for Model Fitting with Applications to Image Analysis and Automated Cartography. *Commun. ACM* **1981**, *24*, 381–395. [CrossRef]
34. Hall, D.K.; Riggs, G.A. *MODIS/Aqua Snow Cover Daily L3 Global 500m SIN Grid, Version 6. [h18v04]*; Technical Report; MYD10A1.006; NASA National Snow and Ice Data Center Distributed Active Archive Center: Boulder, CO, USA, 2016. [CrossRef]
35. Hall, D.K.; Riggs, G.A. *MODIS/Terra Snow Cover Daily L3 Global 500m SIN Grid, Version 6. [h18v04]*; Technical Report; MYD10A1.006; NASA National Snow and Ice Data Center Distributed Active Archive Center: Boulder, CO, USA, 2016. [CrossRef]
36. Riggs, G.A.; Hall, D.K.; Roman, M.O. MODIS Snow Products User Guide for Collection 6 (C6). 2016. Available online: https://modis-snow-ice.gsfc.nasa.gov/?c=userguides (accessed on 23 March 2021).
37. Parajka, J.; Blöschl, G. Spatio-temporal combination of MODIS images - Potential for snow cover mapping. *Water Resour. Res.* **2008**, *44*. [CrossRef]
38. Gafurov, A.; Bardossy, A. Hydrology and Earth System Sciences Cloud removal methodology from MODIS snow cover product. *Hydrol. Earth Syst. Sci* **2009**, *13*, 1361–1373. [CrossRef]
39. Paudel, K.P.; Andersen, P. Monitoring snow cover variability in an agropastoral area in the Trans Himalayan region of Nepal using MODIS data with improved cloud removal methodology. *Remote Sens. Environ.* **2011**, *115*, 1234–1246. [CrossRef]
40. Ronco, P.D.; Michele, C.D. Cloud obstruction and snow cover in Alpine areas from MODIS products. *Hydrol. Earth Syst. Sci.* **2014**, *18*, 4579–4600. [CrossRef]
41. Li, X.; Fu, W.; Shen, H.; Huang, C.; Zhang, L. Monitoring snow cover variability (2000–2014) in the Hengduan Mountains based on cloud-removed MODIS products with an adaptive spatio-temporal weighted method. *J. Hydrol.* **2017**, *551*, 314–327. [CrossRef]
42. Zhang, H.; Zhang, F.; Zhang, G.; Che, T.; Yan, W.; Ye, M.; Ma, N. Ground-based evaluation of MODIS snow cover product V6 across China: Implications for the selection of NDSI threshold. *Sci. Total Environ.* **2019**, *651*, 2712–2726. [CrossRef]
43. Hagolle, O.; Huc, M.; Descardins, C.; Auer, S.; Richter, R. MAJA Algorithm Theoretical Basis Document. Available online: http://dx.doi.org/10.5281/zenodo.1209633 (accessed on 19 March 2021).
44. Pan-European High-Resolution Snow & Ice Products (HR-S&I), Algorithm Theoretical Basis Document for Snow Products. Available online: https://land.copernicus.eu/pan-european/biophysical-parameters/high-resolution-snow-and-ice-monitoring/ (accessed on 24 March 2021).
45. Pan-European High-Resolution Snow & Ice Products (HR-S&I), Product User Manual for Snow Products. Available online: https://land.copernicus.eu/pan-european/biophysical-parameters/high-resolution-snow-and-ice-monitoring/ (accessed on 24 March 2021).
46. Federal Office of Topography Swisstopo. DHM25, The Digital Height Model of Switzerland. Available online: https://www.swisstopo.admin.ch/en/geodata/height/dhm25.html (accessed on 15 March 2021).
47. WSL-Institute for Snow and Avalanche Research SLF. Weekly Winter Report 1–31 October 2017. Available online: https://www.slf.ch/de/lawinenbulletin-und-schneesituation/wochen-und-winterberichte/201718/wob-01-31-oktober.html (accessed on 29 March 2021).
48. WSL-Institute for Snow and Avalanche Research SLF. Weekly Winter Report 1–30 November 2017. Available online: https://www.slf.ch/de/lawinenbulletin-und-schneesituation/wochen-und-winterberichte/201718/wob-01-30-november.html (accessed on 29 March 2021).

49. Parajka, J.; Blöschl, G. Hydrology and Earth System Sciences Validation of MODIS snow cover images over Austria. *Hydrol. Earth Syst. Sci* **2006**, *10*, 679–689. [CrossRef]
50. Parajka, J.; Bezak, N.; Burkhart, J.; Hauksson, B.; Holko, L.; Hundecha, Y.; Jenicek, M.; Krajčí, P.; Mangini, W.; Molnar, P.; et al. Modis snowline elevation changes during snowmelt runoff events in Europe. *J. Hydrol. Hydromech.* **2019**, *67*, 101–109. [CrossRef]
51. Arreola-Esquivel, M.; Toxqui-Quitl, C.; Delgadillo-Herrera, M.; Padilla-Vivanco, A.; Ortega-Mendoza, G.; Carbone, A. Non-Binary Snow Index for Multi-Component Surfaces. *Remote Sens.* **2021**, *13*, 2777. [CrossRef]
52. Wang, Y.; Su, J.; Zhai, X.; Meng, F.; Liu, C. Snow Coverage Mapping by Learning from Sentinel-2 Satellite Multispectral Images via Machine Learning Algorithms. *Remote Sens.* **2022**, *14*, 782. [CrossRef]